Time-resolved X-ray Tomography of Gasoline Direct Injection Sprays

Daniel J. Duke, Andrew B. Swantek, Nicholas Sovis, F. Zak Tilocco, Christopher F. Powell
Energy Systems Division, Argonne National Laboratory, Illinois

Alan L. Kastengren, Doğa Gürsoy
X-ray Science Division, Argonne National Laboratory, Illinois

Tekin Biçer
Mathematics and Computer Science Division, Argonne National Laboratory, Illinois

Abstract

Quantitative measurements of direct injection fuel spray density and mixing are difficult to achieve using optical diagnostics, due to the substantial scattering of light and high optical density of the droplet field. For multi-hole sprays, the problem is even more challenging, as it is difficult to isolate a single spray plume along a single line of sight. Time resolved x-ray radiography diagnostics developed at Argonne's Advanced Photon Source have been used for some time to study diesel fuel sprays, as x-rays have high penetrating power in sprays and scatter only weakly. Traditionally, radiography measurements have been conducted along any single line of sight, and have been applied to single-hole and group-hole nozzles with few plumes. In this new work, we extend the technique to multi-hole gasoline direct injection sprays. By taking time-resolved measurements over a raster-scan pattern from multiple lines of sight, we are able to tomographically reconstruct the time-resolved ensemble mean density field in a plane intersecting the spray. Traditional Fourier back-projection methods are not well-suited for this experiment, so a model-based iterative reconstruction algorithm has been employed in this particular application. Three gasoline direct injection sprays with various 6-hole patterns were studied at injection pressures of 100 to 175 bar and atmospheric back pressure, at selected axial positions several mm downstream of the nozzle. These measurements reveal that the sprays are quite unsteady and interact with each other strongly during the early phase of injection. The spray plume cross-sections are very non-uniform, exhibiting small rich regions on the outer sides of the plumes surrounded by much leaner regions on the inner sides. We propose that this may be due to spray-spray interaction, and spray interaction with the nozzle hole counter-bore.

Introduction

The structure of direct injection multi-hole sprays in close proximity to the nozzle play an important role in the pre-ignition mixing process. Investigation of the near-field spray structure is necessary in order to understand the relationship between the nozzle geometry, the initial conditions (ie. injection pressure, ambient conditions) and the resulting mixture preparation.

Direct injection sprays are typically investigated using visible-light diagnostic techniques [1–4]. If the droplet field is dilute enough, laser-based diagnostics may be employed [5, 6]. However, conventional imaging techniques are not particularly well-suited to the near-field region of the spray, due to the large amount of multiple scattering and high optical density of the droplet field [7].

Multi-hole gasoline direct injection (GDI) sprays are particularly difficult to study using conventional techniques. In addition to the problem of multiple scattering, the close proximity of the spray plumes relative to their skew angles and diameters causes them to substantially overlap. This leads to an increased likelihood of spray-spray interaction and makes the identification of individual plumes challenging [8–10].

In the last decade, x-ray diagnostics have seen increasing use in the study of near-field spray dynamics. X-rays scatter only weakly from gas-liquid interfaces and have high penetrating power [11]. The high flux available at synchrotron sources permits sufficiently high spatial and temporal resolution such that the transient dynamics of fuel sprays can be studied using a variety of complementary techniques [12].

Time-resolved x-ray radiography techniques provide quantitative line of sight measurements of fluid density [13]. From a single line of sight, the spray can be raster-scanned through a focused x-ray beam to provide a planar distribution of projected mass [12]. When considering only a single spray plume, a three-dimensional representation of the density distribution may be estimated by solving an analytical function for the mean density using projection data from a small number of viewing angles [14–16]. If the density field is axisymmetric, an Abel inversion may be used to estimate the density distribution, as is done for the case of cavitation in a nominally axisymmetric nozzle [17, 18]. In the case of multi-hole GDI sprays, the close overlapping of the plumes makes reconstruction from a few limited views difficult. The sprays are in such close proximity that spray-spray interactions cannot be neglected and analytic models are unsuitable.

To understand the three-dimensional structure of multi-hole sprays, computed tomography (CT) can be used to obtain planar density distributions [19]. X-ray CT has been used to study fluid flows for some time [20] and has been applied to a range of problems such as flow in porous media [21] and pipe cavitation [22]. In previous applications to large-scale flows, medical or bench-top x-ray CT sources have been used [23, 24]. Recently, Allocca, Marchitto et al. have demonstrated x-ray CT of transient fuel sprays using a benchtop source. They used polycapillary optics to collimate the beam, improving the spatial resolution [25, 26]. Despite these advances, the low flux from benchtop sources is still a limiting factor. Detailed analysis of small transient features in the spray remains difficult owing to low spatial and temporal resolution. As an alternative, well-collimated monochromatic x-rays from a high-flux synchrotron source are ideal for this application.

Synchrotron light has previously been applied to tomography of multi-hole fuel sprays by Liu et al [27–29]. In their experiments, an area detector recorded x-ray radiographs from multiple view angles. The pixel pitch of the area detector limited the spatial resolution to approximately $150\mu m$. By comparison, the time-resolved x-ray radiography measurements presented here use a focused x-ray beam. The increased

flux enables time-resolved measurements, and the focused beam improves the spatial resolution by a factor of thirty ($5\mu m$). Due to these improvements, the spatial resolution and signal to noise ratio are sufficient to permit time-resolved realization of individual injection events, and ensemble statistics (shot to shot variations in density) can be investigated.

In this paper, we present time-resolved tomographic x-ray radiography measurements of three GDI sprays under atmospheric ambient conditions. Density fields are reconstructed at several slices downstream of the nozzle using a specialized emission tomography algorithm [30]. This allows us to identify the individual plumes of the spray, where this is not possible from a single line of sight projection. The data reveal inhomogeneities within individual spray plumes, and unsteady spray-spray interactions.

Experimental Method

The x-ray measurments were conducted at the 7-BM beamline of the Advanced Photon Source (APS) at Argonne National Laboratory. The facility is specifically designed to make time-resolved measurements of multiphase flows, and is described in detail by Kastengren et al [31]. A simplified schematic of the setup is shown in Fig. 1.

Each of the three fuel injectors studied were supplied with gasoline-type calibration fluid at constant pressure using a piston-accumulator pressurized by regulated inert gas. Each injector was placed in a rotating tomography chamber with thin Kapton windows to permit transmission of the x-ray beam. The chamber was pressurized to approximately 1.2 bar abs at room temperature. A continuous purge flow of nitrogen gas was used to clear droplets from the field of view between each spray event and provide uniform initial conditions.

The x-ray source was a monochromatic beam with mean energy of 8 keV, a bandpass of 1.4% full width at half-maximum (FWHM) and a flux of approximately 2.5×10^{11} ph/s/mm^2. The beam was focused to a spot size of 5×6 μm FWHM with a pair of 300 mm, Rh-coated Kirkpatrick-Baez mirrors. The focused beam acts as a microprobe, allowing a small area to be probed along a line of sight. The experiment was traversed through the fixed beam.

Before the beam interacted with the experiment, it passed through an intensity monitor $I_0(x, y, \theta, t)$ correcting for fluctuations in the incoming beam. The experiment was placed 36.5m downstream from the source; the detector was approximately 10cm down-
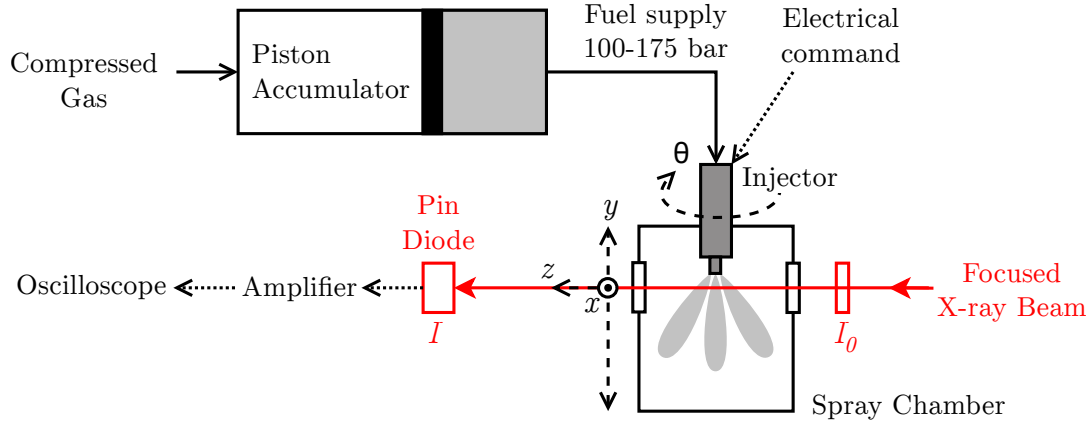
Figure 1: Schematic of x-ray radiography setup for GDI tomography experiments. Note the co-ordinate system (x, y, z) where x is pointing out of the page, y is along the injector body axis, and z is parallel to the x-ray beam. The rotation angle θ is defined with respect to the injector body axis.
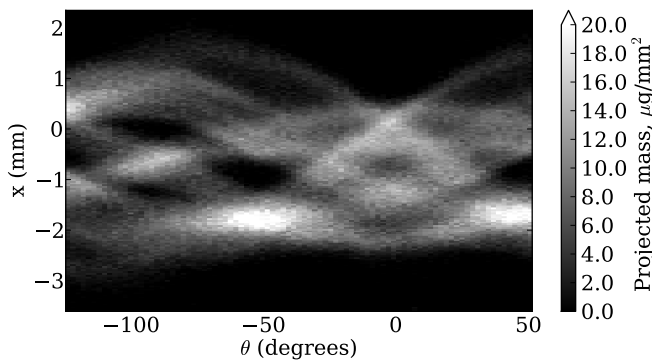

Figure 2: Sinogram of ensemble average projected density for Injector A at $y = 2$mm from the nozzle.

stream of the experiment. The beam passed through the Kapton windows and spray chamber, and was collected by a 300 μm thick PIN diode, providing a measurement of transmitted intensity $I(x, y, \theta, t)$. The amplified transmission signal was sampled at 20 MHz. The signal was integrated over each synchrotron orbit period, giving a temporal resolution of 3.68 μs. The signal to noise ratio of individual injection events was sufficient to allow multiple injections to be individually recored at each sample point for post-hoc statistical analysis.

The transmission signal was normalized by the intensity prior to the arrival of the spray, thus cancelling out the absorption in the ambient chamber gas, windows, and air gap. Using the Lambert-Beer law, the projected mass in the line of sight of the beam due to the spray (M, μg/mm^2) is given as

$$M(x, y, \theta, t) = -\frac{1}{\mu} \log \left[\frac{I(x, y, \theta, t)}{I_0(x, y, \theta, t)} \right] \quad (1)$$

where μ is the attenuation coefficient of the fuel, which is determined by calibration in a cuvette. The projec-

tions $M(x, y, \theta, t)$ are equivalent to the line of sight integral of the density field ρ, μg/mm^3 averaged at each point over the beam spot size A;

$$M(x, y, \theta, t) = \frac{1}{A} \iint \rho(x, y, z, \theta, t)\, dz\, dA. \quad (2)$$

As per Fig. 1, the translation axis x is orthogonal to the injector body axis and y is along the injector body axis. The line of sight of the x-ray beam is in the z axis, and the nozzle rotation θ is aligned with the geometric center of the nozzle holes, which is not always coincident with the injector body axis. The system (x, y, z) is fixed with respect to the x-ray beam, We also define a co-ordinate system (x', y, z') fixed to the injector, such that z is parallel to the electrical connector on the injector body. A set of raster-scan measurements with a sample resolution of 35-75 μm was collected for each θ and the injector was rotated, producing a time-resolved projected density sinogram in a single y-plane, as shown in Fig. 2. These sinograms were reconstructed to retrieve the time-resolved planar density field $\rho(x', z', t)$.

Repeating the measurements N times per sample point gives an ensemble-mean projected density field $\overline{M}(x, y, \theta, t)$, which is reconstructed to provide the ensemble-average density field $\overline{\rho}(x', z', t)$. Similarly, the sample standard deviation $\sigma_M(x, y, \theta, t)$ is reconstructed to provide $\sigma_\rho(x', z', t)$, which gives an indication of the spatial distribution of shot-to-shot variation over a set of injection events. Since both $\sigma_\rho \geq 0$ and $\overline{\rho} \geq 0$ at all points in the (x', z') plane, the same reconstruction method can be applied to both σ_M and $\overline{M}$; σ_ρ represents the planar distribution of standard deviation that best explains the projected values σ_M. Since there is a possibility of a non-normal distribution in σ_M, σ_ρ may contain some systematic error, and cannot be assumed to represent a precise quantitative
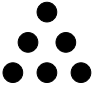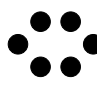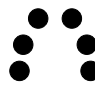
	Injector A	Injector B	Injector C
Make/Model	Bosch HDEV 5 GDI	Bosch HDEV 5 GDI	Bosch HDEV 5 GDI
No. holes	6	6	6
Hole geometry	stepped counterbore	stepped counterbore	stepped counterbore
Skew angle (center of hole pattern)	22°	22°	0°
Injection pressure	100 bar abs	175 bar abs	100 bar abs
Ambient pressure	1.2 bar abs	1.2 bar abs	1.2 bar abs
Commanded injection	1 ms	1 ms	5 ms
Fuel	Gasoline-type calibration fluid	Gasoline-type calibration fluid	Gasoline-type calibration fluid w/400ppm Br additive
Hole pattern	(hole pattern diagram)	(hole pattern diagram)	(hole pattern diagram)

Table 1: Injector geometries and operating conditions for the three cases considered in this study.

local standard deviation. However, σ_ρ does provide a relative indication of the areas in the spray that are most likely to be variable and best explain the shot-to-shot variations in the projections.

Tomographic Reconstruction

We used a penalized-maximum likelihood (PML) approach to reconstruct internal distribution of densities from time-resolved tomographic datasets. The PML algorithm outperforms conventional filtered back-projection algorithms, and is particularly well suited for this application because of its ability to deal with experimental noise and outliers. With the PML approach, rather than maximizing the data-likelihood alone, an additional penalty term is used to enforce desired (e.g. smoothness, sharpness) and/or certain (e.g. non-negativity) properties of the solution [32]. This approach leads to objective functions that combine data misfit and penalty terms, which can be optimized using various iterative and global search methods. This provides a higher-quality reconstruction, particularly for spatio-temporal datasets where the spatial and temporal density gradients are physically bounded. The reconstructions presented here are performed using the open-source software *TomoPy* [30]. The reconstructions were performed on Mira, a 10-petaflops IBM Blue Gene/Q system at Argonne National Laboratory. We used up to 512 nodes where each node consists of 16 physical cores (8192 cores in total) and 16 GiB memory.

Results

Specifications for the three injectors considered in this study are shown in Table 1. All injectors were operated at non-evaporating conditions; 1.2 bar absolute pressure at 25°C, with a proprietary low-volatility gasoline surrogate. For Injector C, 400ppm of tetrabromomethane was blended in the fuel as a contrast agent; this did not notably affect the viscosity or density of the fuel. Injection pressures varied from 100 to 175 bar abs.

Time-resolved measurements of projected spray density were first taken over a single plane for each injector, over a large field of view. Ensemble-average measurements of $N = 32$ injection events were obtained. The time averaged projected mass during the steady phase of injection is shown in Fig. 3 for all three injectors. Regardless of the projection angle, it is not possible to view any of the spray plumes without overlap.

In the time-resolved data, weak fluctuations in the spray plumes are observed, particularly during the first few hundred milliseconds of the injection event. The nature of these fluctuations cannot easily be determined from a projected view (*see supplementary movies* - http://goo.gl/MrBdih). For injector C, Fig. 3c suggests that the lower pair of plumes which are less obscured may be bifurcating, but since they are superimposed, this cannot be directly determined.

Tomographic reconstructions at $y = 2$mm from the nozzle for injector A are shown in Fig. 4. In all the reconstructions, the (x', z') plane is oriented so that

(a) Injector A
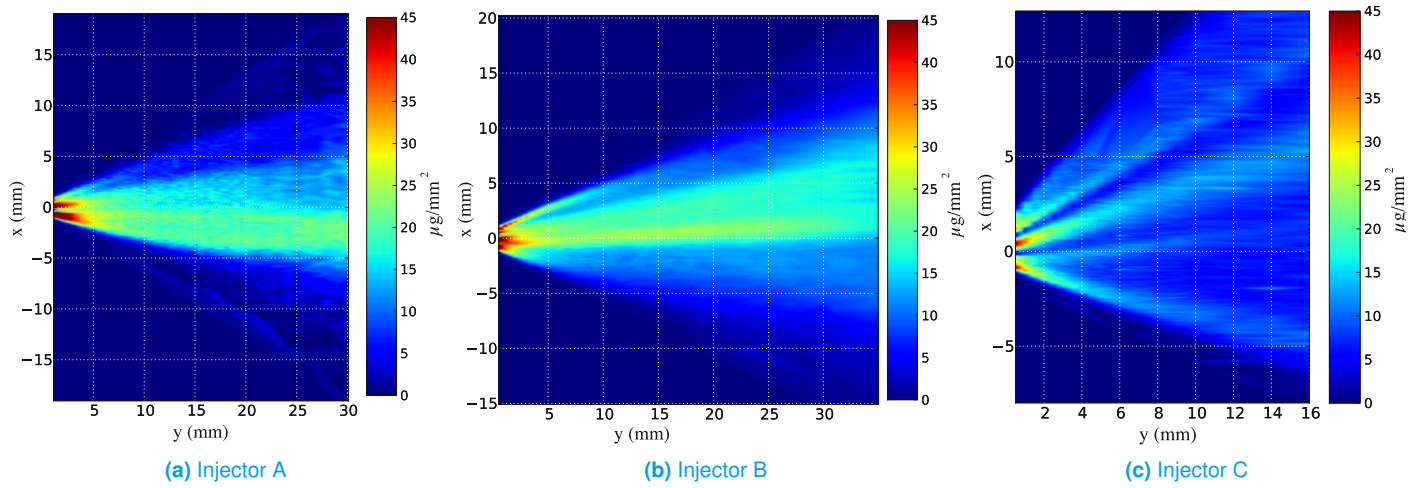
(b) Injector B

(c) Injector C

Figure 3: Radiography measurements of GDI injector mass distribution projected from a single view angle. The data are time-averaged over the steady-state part of the injection, and ensemble-averaged over $N = 32$ events per sample point. Direction of fuel flow is left to right.
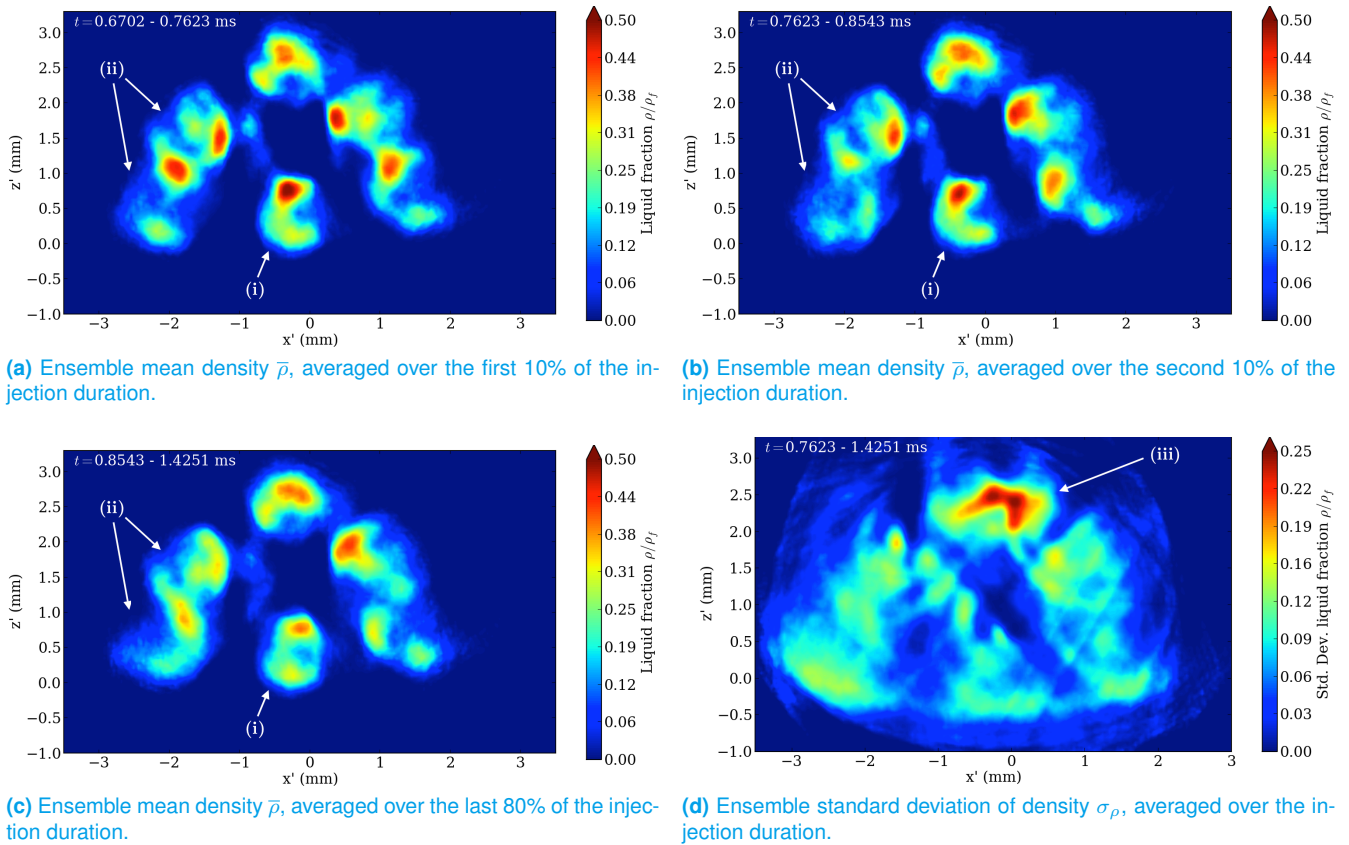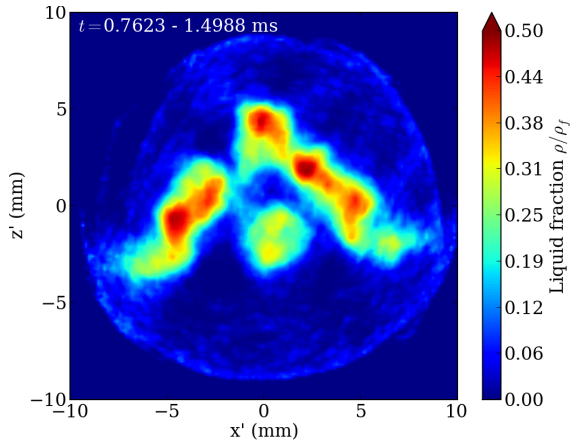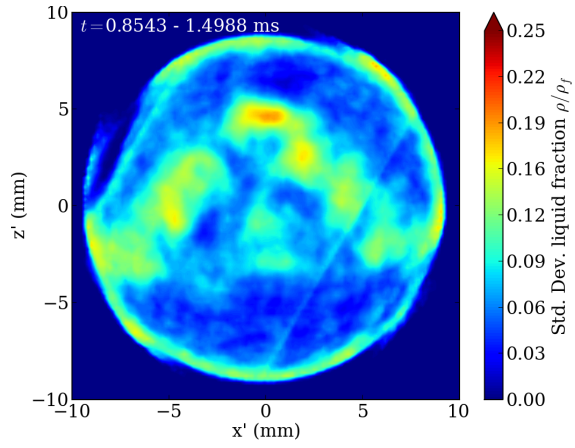

(a) Ensemble mean density $\overline{\rho}$, averaged over the first 10% of the injection duration.

(b) Ensemble mean density $\overline{\rho}$, averaged over the second 10% of the injection duration.

(c) Ensemble mean density $\overline{\rho}$, averaged over the last 80% of the injection duration.

(d) Ensemble standard deviation of density σ_ρ, averaged over the injection duration.

Figure 4: Tomographic reconstructions of injector A at $y = 2$mm from the nozzle.

(a) Ensemble mean density $\bar{\rho}$, averaged over the injection duration.

(b) Ensemble standard deviation of density σ_ρ, averaged over the injection duration.

Figure 5: Tomographic reconstructions of injector A at $y = 10$mm from the nozzle.

the spray is coming out of the page, and the units of density are expressed as a fraction of the fuel density at standard conditions, $\rho_f = 0.7734$ g/cm^3. Since the spray is unsteady during the first 200 μs (20%) of the injection event, the reconstructions have been temporally averaged over several time ranges. Figures 4a-4c show the progression of injector A's mass distribution during the first 10%, second 10% and final 80% of the injection event. It should be noted that since these are the ensemble average of $N = 16$ injection events per sample point, the distributions here represent the mean spray behaviour over several hundred thousand individual injections.

The first point of note in Fig. 4 is the shape of the spray plumes. Rather than being axisymmetric jets, the sprays are typically crescent shaped or highly skewed, with their center of mass typically near the edge of the plume rather than the geometric center. The plume denoted *(i)* in figs. 4a-4c is a good example of a crescent-shaped spray. Most of the spray's mass is located in the upper part of the crescent, and the geometric center is deficient in density.

The second point of note is the unsteady interaction of adjacent spray plumes. The features denoted *(ii)* in figs. 4a-4c are a prime example. Early in the injection, the leftmost lower plume is merging with the plume above it, giving three distinct centers of mass from two nozzle holes (fig. 4a). As the injection event progresses, these jets begin to separate (fig. 4b) until the plumes assume crescent shapes like their neighbors, and can be independently distinguished (fig 4c).

The merging of spray plumes further downstream is interesting, as the spray plumes do not appear to merge due to overlapping as they naturally expand.

Rather, the high-density cores of the plumes become attracted to one another and form large connected regions of high density. This is most evident on the right-hand side of Fig. 5. Since this merging results in large regions of poorly-mixed fuel, it is possible that spray plume merging may be detrimental to spray atomization.

We also note that the contours of lowest density above the noise floor tend to be connected between the plumes, such that no plume is completely surrounded by an unambiguous zero-density region. This is most evident for plume *(i)* in fig. 4. These nonzero low-density regions may represent regions where the sprays meet and droplet collisions are likely to occur, raising the local mean density.

Figure 4d shows the reconstruction of the ensemble standard deviation of the density field during the quasi-steady part of the spray for injector A at $y = 2$mm, averaged over the entire injection duration. Higher values represent larger shot-to-shot variation. Interestingly, we note that the upper plume *(iii)* has triple the standard deviation of the other plumes. This suggests that there are large fluctuations in the amount of injected mass in this plume. Although the other plumes exhibit strong temporal fluctuations, their behavior is more repeatable from shot to shot.

Tomographic measurements were also taken for injector A in a second plane, $y = 10$mm downstream from the nozzle. The time-average ensemble mean density and ensemble standard deviation of the density are shown in Fig. 5. As the spray spreads, many of the local inhomogeneities disappear. In particular, the crescent profiles of the individual plumes give way to more typical solid-core spray jets. The jets are sub-
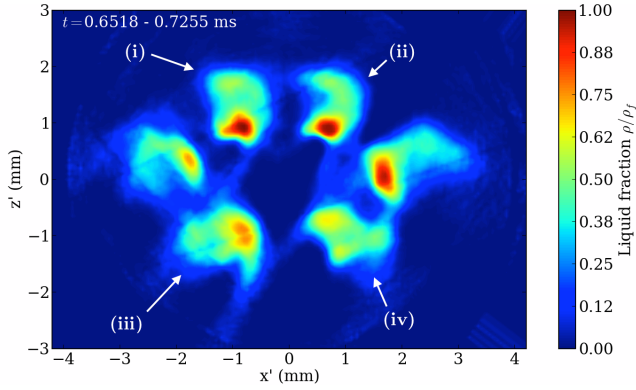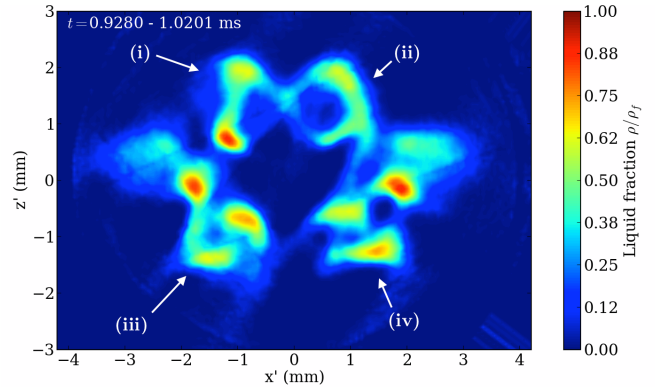
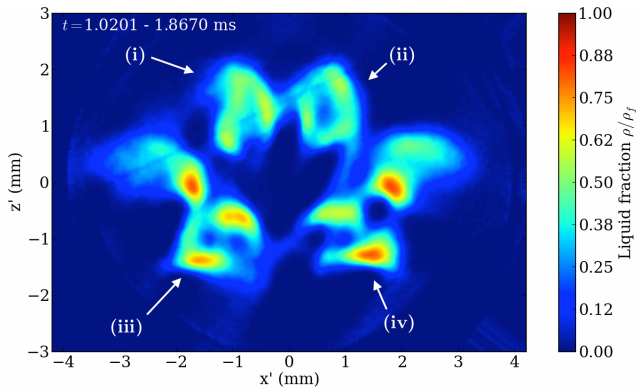**(a)** Ensemble mean density $\overline{\rho}$, averaged over the first 7% of the injection duration.
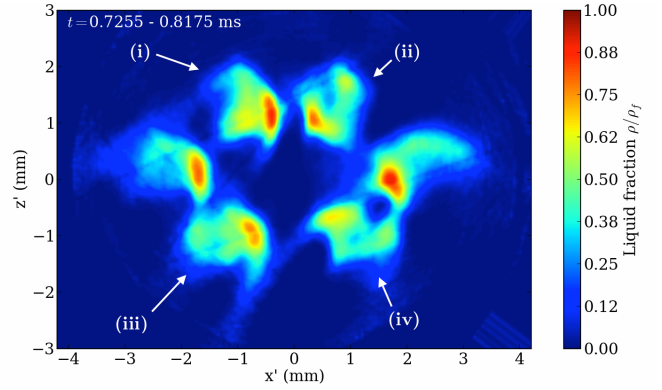
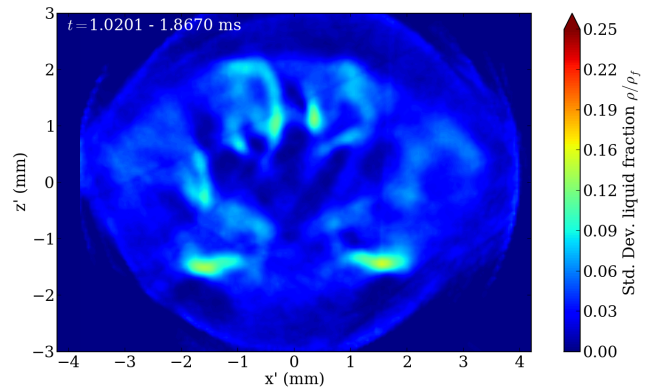**(b)** Ensemble mean density $\overline{\rho}$, averaged the second 7% of the injection duration.
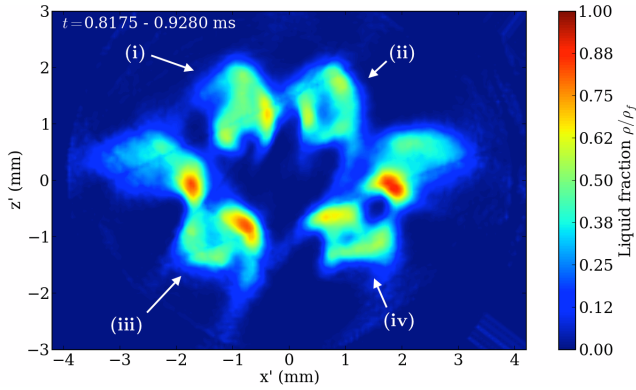
(c) Ensemble mean density $\overline{\rho}$, averaged over the third 7% of the injection duration.

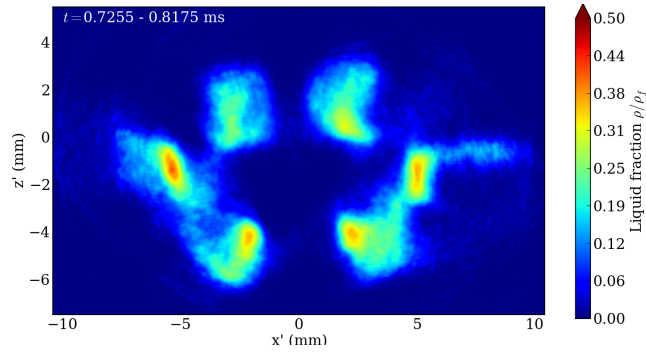**(d)** Ensemble mean density $\overline{\rho}$, averaged over the fourth 7% of the injection duration.

(e) Ensemble mean density $\overline{\rho}$, averaged over the last 69% of the injection duration.
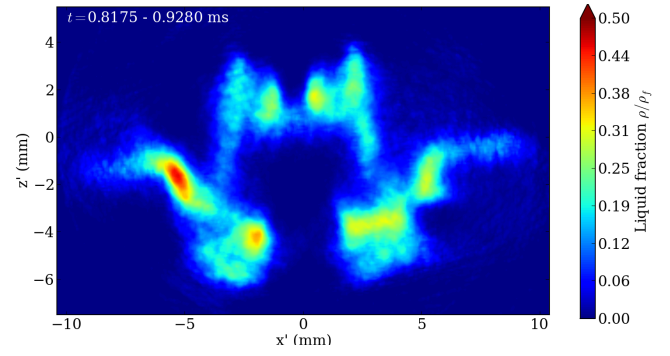
(f) Ensemble standard deviation of density σ_ρ, averaged over the last 69% of the injection duration.
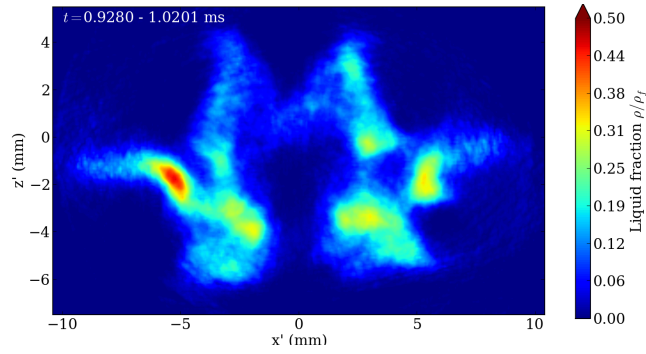
Figure 6: Tomographic reconstructions of injector B at $y = 2$mm from the nozzle.

(a) Ensemble mean density $\overline{\rho}$, averaged over the first 15% of the injection duration.

(b) Ensemble mean density $\overline{\rho}$, averaged over 15-24% of the injection duration.

(c) Ensemble mean density $\overline{\rho}$, averaged over 24-32% of the injection duration.

(d) Ensemble mean density $\overline{\rho}$, averaged over the last 68% of the injection duration.

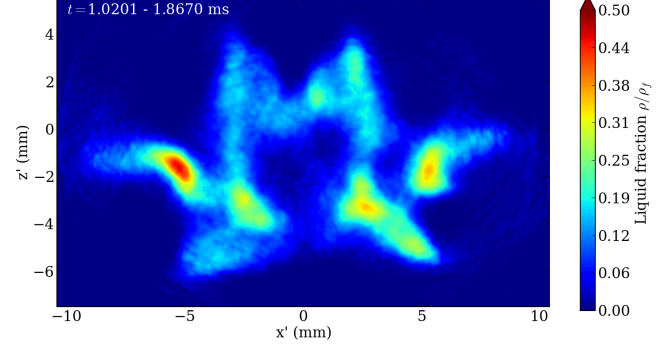**Figure 7:** Tomographic reconstructions of injector B at $y = 10$mm from the nozzle.

stantially merged at this distance; the lower sets of plumes cannot be independently distinguished.

Reconstructions of injector B are shown in Figs. 6 & 7, also at $y = 2$ and 10mm downstream. As for injector A, the sprays are unsteady during the start of the injection event, and become steadier as time progresses. However, in the case of injector B, the unsteadiess is stronger and lasts for about a third of the injection duration.

At the start of injection, the injector B plumes denoted *(i)-(iv)* are solid and separated, but asymmetric (fig 6a). As time progresses, plumes *(i)-(ii)* become crescent-shaped. Initially, plumes *(i)-(ii)* have their center of mass located below their geometric centers, and as time progresses, the centers of mass move toward one another. After approximately 300 μs has elapsed, plumes *(i)-(ii)* undergo a rapid change in shape. The centers of mass between each spray begin to merge, and within less than 100 μs, the sprays suddenly spread outward, and their centers of mass move to the opposite sides (fig 6d). Following this change, the plumes slowly return to their previous crescent shapes (fig 6e).

As for plumes *(iii)-(iv)*, they take the form of asymmet-

ric hollow cones (fig 6b-6c). As time progresses, they transition from crescent shapes to being completely bifurcated (fig 6e). The standard deviation data (fig 6f) show that most of the shot-to-shot variation for injector B may be explained by the variations in the upper and lower plumes. Measurements conducted at $y = 10$mm (fig. 7) show similar behavior. Unlike the case of injector A, injector B's spray plumes maintain their nonuniform shapes much further downstream.

Tomographic reconstructions of injector C are shown in Fig. 8, at $y = 2$mm from the nozzle. Unlike the previous two cases, Injector C's plumes have solid cores. However, as with the other injectors the sprays are highly asymmetric, with the plumes' centers of mass being located closer to the injector body axis than the geometric centers. Merging behavior is also observed for the lower plumes, denoted *(i)-(ii)*. At the start of injection, each plume can be independently distinguished (fig 8a). 200 μs later, the lower pair of plumes begin to be attracted to the plumes above (fig 8b). After 300 μs, plumes *(i)-(ii)* have bifurcated. This bifurcation is also evident in the single-view radiography data (Fig 3c). The peak density regions do not merge completely with the central plumes, but are close enough that there is no region of zero spray density between them.

Discussion

Several interesting findings arise from the tomography data. Firstly, we note that for two of the three injectors, the sprays plumes are often hollow, having a cone or crescent shape. For all the injectors, the spray plumes are asymmetric, resulting in an uneven mass distribution across the spray. We propose that these structures may result from interaction of the spray with the nozzle counterbore. Since the ambient pressure is relatively low, the spray spreading angle may be large enough that the spray impinges on the counterbore wall. This will act to redirect some of the spray in a roughly conical shape around the plume due to coalescence. The deceleration of the fluid due to impingement will locally inhibit atomization. The skew angle of the hole relative to the velocity vector of the exiting fluid will determine to a large extent which side of the counterbore experiences impingement. Modelling studies have shown the importance of recirculation and entrainment inside the counterbore [33, 34]; this may also promote the formation of crescent-shaped spray plumes.

Another finding from this study is that unsteady spray-spray interaction is a significant factor in spray mixing in the near-nozzle region. The formation of asymmetric, hollow-cone and crescent-shaped sprays will promote additional interaction, as most of each plume's mass is located on its periphery, close to the adjacent plumes. These two effects are likely to be coupled. The proximity of high-density regions can lead to complex interactions such as merging and bifurcation. On occasion, fuel jets may reflect rather than merge, and be driven apart (fig 6d). Merging, birfurcating and reflecting jet behaviour is an active area of research in low-speed flows [35,36], but is not yet well understood in high-pressure sprays. We observe that peripheral plumes with larger skew angles are qualitatively more subject to bifurcation and merging.

Finally, analysis of the ensemble standard deviation fields shows that the shot to shot variation is not always consistent between spray plumes. For injector A, the upper plume showed a significantly larger shot to shot variation than the other holes, whilst for injector B, the shot to shot variation was much more uniform. A further investigation of the nozzle internal flow is required to understand this phenomenon.

Conclusions

In this paper, we have undertaken a preliminary study of the fuel density distribution in multi-hole GDI sprays using time-resolved x-ray tomography. X-ray radiography permits the investigation of near-nozzle fuel spray
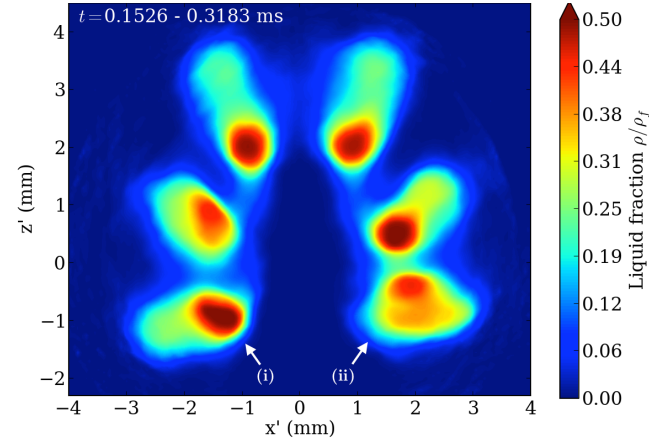
(a) Ensemble mean density $\overline{\rho}$, averaged over the first 3.5% of the injection duration.
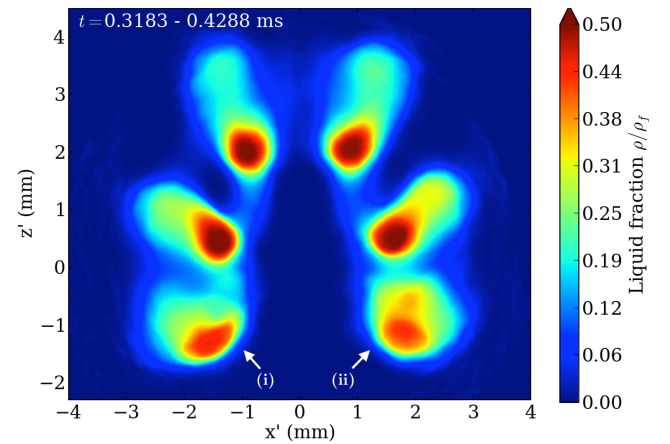
(b) Ensemble mean density $\overline{\rho}$, averaged over 3.5-6% of the injection duration.
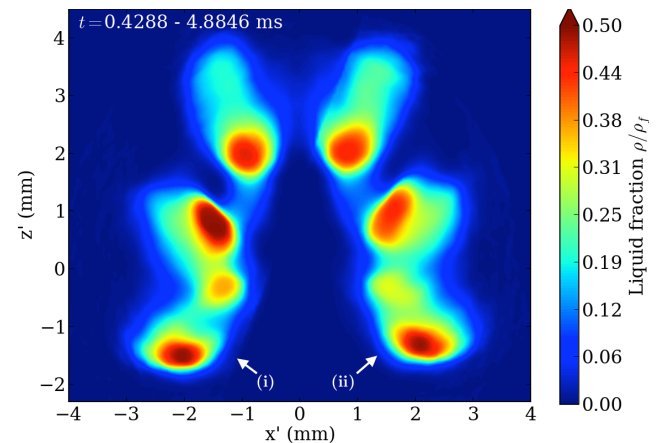
(c) Ensemble mean density $\overline{\rho}$, averaged over the last 94% of the injection duration.

Figure 8: Tomographic reconstructions of injector C at $y = 2$mm from the nozzle.

structures, and the application of CT reveals details of spray structure and interaction that are not apparent from visible-light imaging nor x-ray radiography from a single view.

Under a limited set of conditions and at non-evaporating atmospheric ambient conditions, several interesting features are observed. Unlike the nozzle holes, the spray plumes are neither uniform nor axisymmetric, tending to either be jets with a skewed center of mass, crescents, or hollow cones. We propose that this may be due to spray interaction with the nozzle hole counterbore.

Unsteadiness in the projected density is explained by structural changes in the plumes as they interact with one another. In some circumstances, spray plumes are attracted to one another and merge. In some cases, the plume will bifurcate, with one jet merging with its neighbour. In this configuration, it is possible to have three spray plumes issuing from only two nozzle holes. In other cases, spray interaction causes the plumes to repel from one another for a short time. These spray interactions are unsteady, and are observed most often in the outermost plumes with larger skew angles.

For the set of injector geometries considered here, the unsteadiness in spray structure tends to persist over the first 20-40% of the injection, before reaching a steady state. The unsteadiness in density distribution and plume structure are persistent from shot to shot and are clearly visible in the ensemble mean density fields; they are not occasional occurences.

Investigation of the shot-to-shot variation via reconstruction of the ensemble standard deviation show that the shot-to-shot variation in GDI sprays is not always evenly distributed. For some geometries, a single hole can account for a substantial fraction of the standard deviation in projected density. This may be due to variations in internal flow, which in turn depend on the hole arrangement and geometry.

The physical mechanisms underlying phenomena such as spray-spray interaction, spray plume shape and spray instability are complex and not yet fully understood. Internal flow dynamics, entrainment and wall interaction in the counterbore region and hydrodynamic interactions between spray plumes are all likely to play a role in explaining these phenomena, and are matters for further investigation.

References

[1] G M Faeth, L Hsiang, and P Wu. Structure and breakup properties of sprays. Int. J. Multiphas. Flow, 21:99–127, 1995.

[2] J Kostas, D Honnery, J Soria, A Kastengren, Z Liu, C F Powell, and J Wang. Effect of nozzle transients and compressibility on the penetration of fuel sprays. Appl. Phys. Lett., 95:024101, 2009.

[3] P G Aleiferis, J Serras-Pereira, Z van Romunde, J Caine, and M Wirth. Mechanisms of spray formation and combustion from a multi-hole injector with E85 and gasoline. Combustion and Flame, 157(4):735–756, 2010.

[4] Mark Linne. Imaging in the optically dense regions of a spray: A review of developing techniques. Progress in Energy and Combustion Science, 39(5):403–440, 2013.

[5] N Mitroglou, J M Nouri, and M Gavaises. Spray characteristics of a multi-hole injector for direct-injection gasoline engines. Int. J. Engine. Res., 7:255–270, 2006.

[6] N Mitroglou, J M Nouri, Y Yan, M Gavaises, and C Arcoumanis. Spray Structure Generated by Multi-Hole Injectors for Gasoline Direct-Injection Engines. SAE Paper 2007-01-1417, April 2007.

[7] J S Lee, B M Weon, and J H Je. X-ray phase-contrast imaging of dynamics of complex fluids. J. Phys. D: Appl. Phys, 46(49):494006, 2013.

[8] S Park, H Cho, I Yoon, and K Min. Measurement of droplet size distribution of gasoline direct injection spray by droplet generator and planar image technique. Meas. Sci. Technol., 13(6):859–864, 2002.

[9] F Beyrau, A Brauer, T Seeger, and A Leipertz. Gas-phase temperature measurement in the vaporizing spray of a gasoline direct-injection injector by use of pure rotational coherent anti-Stokes Raman scattering. Optics Letters, 29(3):247–249, 2004.

[10] M Yamakawa, D Takaki, T Li, Y Y Zhang, and K Nishida. Quantitative Measurement of Liquid and Vapor Phase Concentration Distributions in a D.I. Gasoline Spray by the Laser Absorption Scattering (LAS) Technique. SAE Paper 2002-01-1644, 2002.

[11] Theodore J Heindel. A Review of X-Ray Flow Visualization With Applications to Multiphase Flows. J. Fluids Eng., 133(7):074001, 2011.

[12] Alan Kastengren and Christopher F Powell. Synchrotron X-ray techniques for fluid dynamics. Exp. Fluids, 55(3):1686, 2014.

[13] W Cai, C F Powell, Y Yue, S Narayanan, J Wang, M W Tate, M J Renzi, A Ercan, E Fontes, and S M Gruner. Quantitative analysis of highly transient fuel sprays by time-resolved x-radiography. Appl. Phys. Lett., 83(8):1671–1673, 2003.

[14] A Kastengren, C F Powell, Z Liu, and J Wang. Time resolved, three dimensional mass distribution of diesel sprays measured with X-ray radiography. SAE Paper 2009-01-840, 2009.

[15] A Kastengren, C Powell, Z Liu, S Moon, J Gao, X Zhang, and J Wang. Axial Development of Diesel Sprays at Varying Ambient Density. In Proceedings of ILASS Americas, 22nd Annual Conference on Liquid Atomization and Spray Systems, Cincinnati, OH, March 2010.

[16] A L Kastengren, F Tilocco, D Duke, C Powell, X Zhang, and S Moon. Time-Resolved X-Ray Radiography of Sprays from Engine Combustion Network Spray A Diesel Injectors . Atom. Sprays, 24(3):251–272, 2014.

[17] D Duke, A L Kastengren, F Tilocco, A B Swantek, and C F Powell. X-ray Radiography Measurements of Cavitating Nozzle Flow. Atom. Sprays, 23(9):841–860, 2013.

[18] D J Duke, A B Swantek, Z F Tilocco, A L Kastengren, K Fezzaa, K Neroorkar, M Moulai, C F Powell, and D P Schmidt. X-ray Imaging of Cavitation in Diesel Injectors. SAE Int. J. Engines, 7(2):1003–1016, 2014.

[19] A Kak and M Slaney. Principles of Computerized Tomographic Imaging. In Principles of Computerized Tomographic Imaging. IEEE Press, New York, 1999.

[20] R L Powell. Experimental techniques for multiphase flows. Phys. Fluids, 20:040605, 2008.

[21] W P Breugem, V van Dijk, and R Delfos. Flows Through Real Porous Media: X-Ray Computed Tomography, Experiments, and Numerical Simulations. J. Fluids Eng., 136(4):040902, 2014.

[22] D Bauer, H Chaves, and C Arcoumanis. Measurements of void fraction distribution in cavitating pipe flow using x-ray CT. Meas. Sci. Technol., 23(5):055302, 2012.

[23] B R Halls, T J Heindel, A L Kastengren, and T R Meyer. Evaluation of X-ray sources for quantitative two- and three-dimensional imag- ing of liquid mass distribution in atomizing sprays. Int. J. Multiphas. Flow, 59(C):113–120, 2013.

[24] B Halls, C Radke, T Heindel, W Lohry, S Zhang, T Meyer, M Lightfoot, S Danczyk, S Schumaker, S Roy, J Gord, and A L Kastengren. Characterization of three-dimensional dense spray visualization techniques. In 51st AIAA Aerospace Sciences Meeting including the New Horizons Forum and Aerospace Exposition, Reston, Viriginia, January 2013. American Institute of Aeronautics and Astronautics.

[25] L Marchitto, S B Dabagov, L Allocca, D Hampai, A Liedl, and S Alfuso. X-ray tomography of high pressure fuel spray by polycapillary optics. In A Khounsary, S Goto, and C Morawe, editors, Advances in X-Ray/EUV Optics and Components VIII, Proc. of SPIE, volume 8848. SPIE, 2013.

[26] L Allocca, S Alfuso, L Marchitto, D Hampai, and S Dabagov. Spatial analysis of fuel density from automotive transient sprays by polycapillary x-ray imaging. In Proceedings of ICLASS 2012, 12th Triennial International Conference on Liquid Atomization and Spray Systems, Heidelberg, Germany, September 2012.

[27] X Liu, J Liu, X Li, and S K Cheong. Development of ultrafast computed tomography of highly transient fuel sprays. In Proc. SPIE, volume 5535, 2004.

[28] X Liu, K S Im, Y Wang, J Wang, D L S Hung, J R Winkelman, M W Tate, A Ercan, L J Koerner, T Caswell, D Chamberlain, D R Schuette, H Philipp, D M Smilgies, and S M Gruner. Quantitative Characterization of Near-Field Fuel Sprays by Multi-Orifice Direct Injection Using Ultrafast X-Tomography Technique. SAE Paper 2006-01-1041, 2006.

[29] X Liu, K S Im, Y Wang, J Wang, M W Tate, A Ercan, D R Schuette, and S M Gruner. Four dimensional visualization of highly transient fuel sprays by microsecond quantitative x-ray tomography. Appl. Phys. Lett., 94(8):084101–084101, 2009.

[30] D Gursoy, F De Carlo, X Xiao, and C Jacobsen. TomoPy: a framework for the analysis of synchrotron tomographic data. J. Synchrotron Rad., 21:1188–1193, 2014.

[31] A L Kastengren, C F Powell, D Arms, E M Dufresne, H Gibson, and J Wang. The 7BM beamline at the APS: a facility for time-resolved fluid dynamics measurements. J Synchrotron Rad., 19(4):654–657, 2012.

[32] J Kaipo and E Somersalo. Springer, New York, NY, 2004.

[33] B Befrui, G Corbinelli, P Spiekermann, M Shost, and M C Lai. Large eddy simulation of GDi single-hole flow and near-field spray. SAE Paper, 2011-01-1211, 2012.

[34] M A Shost, M C Lai, B Befrui, P Spiekermann, and D L Varble. GDi Nozzle Parameter Studies Using LES and Spray Imaging Methods. SAE Paper, 2014-01-1434, 2014.

[35] J W M Bush and A E Hasha. On the collision of laminar jets: fluid chains and fishbones. J. Fluid Mech., 2004.

[36] M Thrasher, S Jung, Y Pang, C P Chuu, and H Swinney. Bouncing jet: A Newtonian liquid rebounding off a free surface. Phys. Rev. E, 76(5):056319, 2007.